

Maskless fabrication of quasi-omnidirectional V-groove solar cells using an alkaline solution-based method

Xingqian Chen(陈兴谦), Yan Wang(王燕), Wei Chen(陈伟), Yaoping Liu(刘尧平), Guoguang Xing(邢国光), Bowen Feng(冯博文), Haozhen Li(李昊臻), Zongheng Sun(孙纵横), and Xiaolong Du(杜小龙)
Citation: Chin. Phys. B, 2024, 33 (**1**): 018801. DOI: 10.1088/1674-1056/ad0cd0
Journal homepage: http://cpb.iphy.ac.cn; http://iopscience.iop.org/cpb

What follows is a list of articles you may be interested in

Dependence of the solar cell performance on nanocarbon/Si heterojunctions

Shiqi Xiao(肖仕奇), Qingxia Fan(范庆霞), Xiaogang Xia(夏晓刚), Zhuojian Xiao(肖卓建), Huiliang Chen(陈辉亮), Wei Xi(席薇), Penghui Chen(陈鹏辉), Junjie Li(李俊杰), Yanchun Wang(王艳春), Huaping Liu(刘华平), Weiya Zhou(周维亚)
Chin. Phys. B, 2018, 27 (**7**): 078801. DOI: 10.1088/1674-1056/27/7/078801

Detection of finger interruptions in silicon solar cells using photoluminescence imaging

Lei Zhang(张磊), Peng Liang(梁鹏), Hui-Shi Zhu(朱慧时), Pei-De Han(韩培德)
Chin. Phys. B, 2018, 27 (**6**): 068801. DOI: 10.1088/1674-1056/27/6/068801

Application of millimeter-sized polymer cylindrical lens array concentrators in solar cells

Yao-Ju Zhang(张耀举), Yi-Jie Li(李艺杰), Jie Lin(林洁), Chao-Long Fang(方朝龙), Si-Yuan Liu(刘思远)
Chin. Phys. B, 2018, 27 (**5**): 058801. DOI: 10.1088/1674-1056/27/5/058801

Improvement in IBC-silicon solar cell performance by insertion of highly doped crystalline layer at heterojunction interfaces

Hadi Bashiri, Mohammad Azim Karami, Shahramm Mohammadnejad
Chin. Phys. B, 2017, 26 (**10**): 108801. DOI: 10.1088/1674-1056/26/10/108801

Boron implanted emitter for n-type silicon solar cell

Liang Peng (梁鹏), Han Pei-De (韩培德), Fan Yu-Jie (范玉洁), Xing Yu-Peng (邢宇鹏)
Chin. Phys. B, 2015, 24 (**3**): 038801. DOI: 10.1088/1674-1056/24/3/038801

RAPID COMMUNICATION

Maskless fabrication of quasi-omnidirectional V-groove solar cells using an alkaline solution-based method

Xingqian Chen(陈兴谦)[1,2,3], Yan Wang(王燕)[1,2,4,†], Wei Chen(陈伟)[2], Yaoping Liu(刘尧平)[1,2,‡], Guoguang Xing(邢国光)[1,2,3], Bowen Feng(冯博文)[1,2,3], Haozhen Li(李昊臻)[1,2,3], Zongheng Sun(孙纵横)[1,2,3], and Xiaolong Du(杜小龙)[1,2,§]

[1] *Beijing National Laboratory for Condensed Matter Physics, Institute of Physics, Chinese Academy of Sciences, Beijing* 100190, *China*
[2] *Songshan Lake Materials Laboratory, Dongguan* 523808, *China*
[3] *School of Physical Sciences, University of Chinese Academy of Sciences, Beijing* 100049, *China*
[4] *Beijing Hairou Laboratory, Beijing* 101400, *China*

(Received 25 September 2023; revised manuscript received 25 October 2023; accepted manuscript online 16 November 2023)

Silicon passivated emitter and rear contact (PERC) solar cells with V-groove texture were fabricated using maskless alkaline solution etching with in-house developed additive. Compared with the traditional pyramid texture, the V-groove texture possesses superior effective minority carrier lifetime, enhanced p–n junction quality and better applied filling factor (FF). In addition, a V-groove texture can greatly reduce the shading area and edge damage of front Ag electrodes when the V-groove direction is parallel to the gridline electrodes. Due to these factors, the V-groove solar cells have a higher efficiency (21.78%) than pyramid solar cells (21.62%). Interestingly, external quantum efficiency (EQE) and reflectance of the V-groove solar cells exhibit a slight decrease when the incident light angle (θ) is increased from 0° to 75°, which confirms the excellent quasi omnidirectionality of the V-groove solar cells. The proposed V-groove solar cell design shows a 2.84% relative enhancement of energy output over traditional pyramid solar cells.

Keywords: V-groove, alkaline etching, quasi omnidirectionality, silicon solar cell

PACS: 88.40.hj, 88.40.H–, 84.60.Rb **DOI:** 10.1088/1674-1056/ad0cd0

1. Introduction

The texture of a monocrystalline silicon (c-Si) solar cell plays an important role in light trapping. Among the various types of textures, the pyramid structure has become the mainstream of current industrial production due to its low cost and high conversion efficiency.[1,2] Although the pyramid structure offers excellent performance under vertically incident light, its antireflection ability deteriorates rapidly with the increase of angle of incidence (AOI).[3] This drawback can be effectively mitigated by employing a photovoltaic sun tracking system but it is generally expensive to ensure the working of c-Si solar cells under vertical light incidence.[4] Therefore, broadband and omnidirectional antireflection capacity of solar cells have been considered in order to obtain consistently higher electrical generation at a broader range of AOI. In addition, in the application of building-integrated photovoltaics (BIPV), broadband and omnidirectional antireflection capacity of solar cells become particularly critical because the position of solar cells usually cannot be changed.

In recent years, several studies have explored the possibility of achieving quasi omnidirectionality of solar cells using different nanotextures.[5–10] For example, Zhong *et al.*[10] reported near zero reflection over AOI of 0°–60° using a Si-nanowire structure, which was attributed to a combination of effects such as the gradient refractive index, light scattering, and Mie resonance of nanotexture. Xu *et al.*[7] reported a Si nano-cone texture obtained by a high-throughput plasma texturizing process that enabled broadband and omnidirectional light-trapping. Spinelli *et al.*[5] demonstrated that Si nanocylinder arrays fabricated by a soft-imprint technique could reduce reflection omnidirectionally over a broad AOI of approximately 0°–60°. Although the aforementioned nanostructures achieved optical optimization, the electrical performance of the solar cells was quite poor due to serious surface recombination effects.[11–14] In this regard, Si nanopyramids texture has shown to significantly reduce the surface area compared with the other nanostructures. However, the traditional micro-pyramid texture still outperforms most texture variants, which implies that micron-sized textures have the added advantage of lower surface recombination.[2]

The micron-sized V-groove structure has excellent quasi-omnidirectional characteristics with fewer surface-hanging bonds, which provides a possibility to balance the optical and electrical performances.[15,16] However, V-groove textures are usually fabricated using complex and expensive processes such as photolithography, which has hindered its development

†Corresponding author. E-mail: wangyan1987@hrl.ac.cn
‡Corresponding author. E-mail: ypliu@iphy.ac.cn
§Corresponding author. E-mail: xldu@iphy.ac.cn

© 2024 Chinese Physical Society and IOP Publishing Ltd

for mass production.[17,18] Other less expensive fabrication methods such as mechanical texturization and laser ablation have a tendency to induce extensive surface damage that significantly deteriorates the performance of the solar cells.[19–21] Recently, the V-groove texture was successfully fabricated on diamond-wire sawn (DWS) c-Si wafers through a one-step Cu-assisted chemical etching, which is compatible with existing production line technology.[15,16] However, the etching solution contains Cu ions which are unsuitable for industrial application and pose an environmental risk. So far, there are no reports of fabricating V-groove texture by typical maskless alkaline solution etching, which is currently the most widely used technology in industry. Although the V-groove structure has been proposed as texture in silicon solar cells,[22,23] quasi-omnidirectional characteristic of the V-groove textured silicon solar cell has not yet been confirmed experimentally.

In this study, V-groove texture was fabricated by maskless alkaline solution etching with the help of natural mask formed on DWS silicon wafer and an in-house developed additive. Compared with typical pyramid texture, V-groove texture was more easily passivated by the SiN_x film due to fewer dangling bonds, thus exhibiting higher minority carrier lifetime and lower surface recombination rate. In addition, the V-groove texture greatly reduced the shading area of the front Ag electrodes by limiting the width of screen-printed Ag fingers, which contributed to superior short-circuit current density (J_{sc}) of the V-groove solar cells. Finally, a higher average efficiency of 21.78% was achieved with V-groove texture, which was 0.14% higher than pyramid textured solar cells. As AOI was increased from 0° to 75°, the external quantum efficiency (EQE) of the V-groove textured solar cells decreased gradually compared to the pyramid textured ones, exhibiting excellent quasi-omnidirectionality. Finally, a 2.68% increment in power generation can be expected every year by evaluating relative enhancement of energy output of the V-groove solar cells compared to pyramid solar cells at Songshan Lake Materials Laboratory.

2. Experimental detials

2.1. Fabrication of texture

For fabrication of V-groove and pyramid textures, (100)-oriented DWS P-type Czochralski (CZ) Si wafers (gallium-doped) with size of 158.75 mm×158.75 mm and a resistivity of 1–3 Ω cm were used as substrates. The V-groove texture was prepared by immersing the silicon wafers in 1.1% KOH alkaline solution containing an in-house developed additive I with hypochlorite and nucleating agent at 70 °C for 480 s, where the hypochlorite can oxidize crystalline silicon rather than amorphous silicon and promote the reaction between crystalline silicon with KOH. The pyramid-textured wafers were obtained by immersing the samples in 1.1% KOH alkaline solution containing a commercial additive II (nucleating and surface activity agents) at 80 °C for 600 s.

The nucleating and surface activity agents used in this work are hydroxypropyl methylcellulose and sodium polyoxymethylene sulfonate, respectively. Hydroxypropyl methylcellulose is a relatively strong nucleating agent that can quickly form nucleation points along saw marks on the surface of silicon wafers. And sodium polyoxymethylene sulfonate acts as nucleation conditioner, and due to its strong dispersibility, it can evenly distribute the solution on the surface of the silicon wafer, making the reaction process more uniform. In addition, the hypochlorite can increase the difference in etching rate between amorphous silicon and crystalline silicon, which plays a crucial role in the formation of V-groove texture.

2.2. Fabrication of PERC solar cells

The standard fabrication process for industrial solar cells was adopted to prepare the textured silicon wafers into PERC solar cells, which included P thermal diffusion on the front side to form p–n junction, local doping by laser for front electrode contact, back polishing in HNO_3/HF mixed solution, removal of the front phosphorous silicate glass (PSG) in dilute HF solution, deposition of SiN_x layers on the front surface by plasma enhanced chemical vapor deposition (PECVD) systems, deposition of Al_2O_3/$SiON_x$ layers on the back surface by atomic layer deposition (ALD) system and PECVD, laser slotting for back electrode contact, and screen printing and co-firing.

2.3. Characterization

Surface morphologies of Si wafers were observed by scanning electron microscope (SEM, Hitachi Regulus 8100, 10 kV) and the corresponding surface layer composition was investigated by a fast micro-confocal Raman imaging system (Horiba LabRam HR Evolution). For the Raman measurement, the laser power was set to 2.6 mW and the spot diameter was 721.15 nm. The integration time was 25 s and all the Raman peaks were calibrated based on 520.7 cm^{-1} of Si. Field-emission transmission electron microscope (TEM, JEOL JEM-F200, 20 kV) was used to study the phases of silicon on the surface, and the cross-sectional TEM samples were prepared by a combined system of focused ion beam (FIB, Hitachi NX5000) and SEM. The reflectance was characterized by an ultraviolet–visible–near infrared absorption spectrometer (Hitachi UH4150) with a xenon lamp. WCT-120 (Sinton) of xenon lamp light source with intensity 1 sun was used to test τ_{eff} and applied FF using quasi-steady generalized (1/1) mode. In addition, quantum efficiencies of the solar cells were measured by a photoelectric test system with a tiltable sample holder.

2.4. Simulations

The optical performance of the samples was simulated by a web-based software called Wafer Ray Tracer hosted by PV Lighthouse. The thickness of silicon wafer was set to 170 μm. The angle, height, and width for both pyramid and V-groove textures were assumed to be 54.74°, 1.41 μm and 2.00 μm, respectively. The thicknesses of SiN_x front coating and $SiON_x$ back coating were 80 nm and 120 nm, respectively. The incident light angle (θ) varied from 0° to 75° to obtain the omnidirectional reflectivity. Solar spectrum irradiances at Songshan Lake Materials Laboratory (latitude of 22.9°, longitude of 113.9°) with different time were acquired from the solar spectrum calculator on the website of PV Lighthouse.

3. Results and discussion

3.1. Fabrication of V-groove texture in alkaline solution

The formation process of V-groove texture is shown in Fig. 1. The surface morphology of raw DWS silicon wafers is divided into two types, namely, flat concave region A and rough convex region B (Fig. 1(a)). After being etched in alkaline solution for 60 s (Fig. 1(b)), region A was etched away while region B remained. With the prolonging of etching time, the edge of region B started to be etched, and gradually formed the ridge of V-groove. Appearance of the V-groove is evident in Fig. 1(c). The final V grooves were formed after etching for 480 s in the alkaline solution (Fig. 1(d)). The width and height of the V-groove are within the range of 1–3 μm. And the tested title angle is 72.7°.

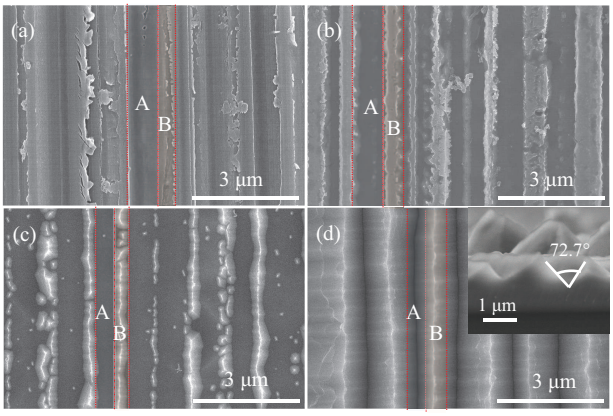


Fig. 1. SEM images of DWS silicon wafers surface before (a) and after etching in alkaline solution for (b) 60 s, (c) 240 s, and (d) 480 s.

In order to investigate the reason for etching rate difference between region A and region B, dynamic Raman spectra were measured to analyze the surface phase change of silicon in these two regions. With the help of SEM, region A and region B were marked for the Raman tests. The Raman spectra of region A and region B with different etching time are shown in Fig. 2. For the original silicon substrate, peaks of amorphous silicon (α-Si) can be observed at 145 cm^{-1}, 300 cm^{-1} and 470 cm^{-1},[24] whereas the R8-structure Si-XII phase is located at 350 cm^{-1}.[24] The wurtzite-structure Si-IV located at 508 cm^{-1} [25] appears in both regions, which originates from the fracture, rotation and reorganization of Si–Si bonds caused by the stress effect during the cutting process. In the Raman spectrum of region A, a special peak is observed at 521 cm^{-1} associated with the diamond cubic structure (Si-I) from the silicon substrate, indicating that the surface layer of region A is thinner compared to that of region B.[25] It has been reported that under a static uniaxial stress of 11.3–12.5 GPa, the diamond-cubic-structure Si-I phase would irreversibly transform into metallic β-Si, namely, Si-II phase, which possesses good ductility and can transfer from region A to region B, and in addition, can completely transform to amorphous silicon under a rapid release of load.[26–28] Thus, the alternately distributed A and B stripes are constituted by α-Si embedded with Si-XII and Si-IV nanocrystals, with B being thicker than A.

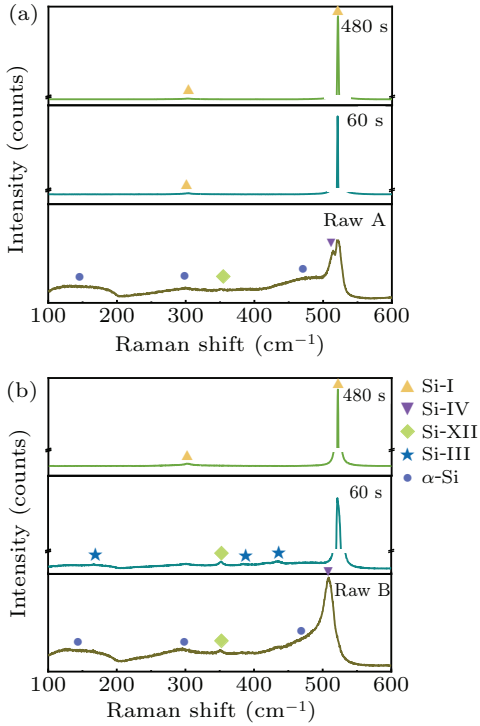


Fig. 2. Raman spectra of (a) region A and (b) region B on DWS silicon wafers surface before and after etching in alkaline solution for 60 s and 480 s.

After etching in alkaline solution for 60 s, surface layer related Raman signals, such as the peaks of amorphous silicon, Si-IV, and Si-XII phases, become weaker in region B and even disappear in region A. In contrast, the Si bulk related peaks, such as those corresponding to the Si-I phase, are enhanced, indicating that the surface layers in these two regions were removed rapidly in the beginning 60 s. The surface layer was completely etched away in region A, while it still existed in region B, which is consistent with the SEM image in Fig. 1(b). Since the etching rate of the (100)-oriented silicon is over 30 times faster than that of amorphous silicon,[29]

the region B can act as a mask whose effect is greatly amplified when the hypochlorite exists. In this case, small pyramids nucleated along region B, and then connected into lines in the process of alkaline etching. Finally, due to the slowest etching rate of {111},[30–32] the lines were surrounded by {111} and gradually grew to grooves. When the grooves formed, the surface layer in region B disappeared, fulfilling its mission as a mask.

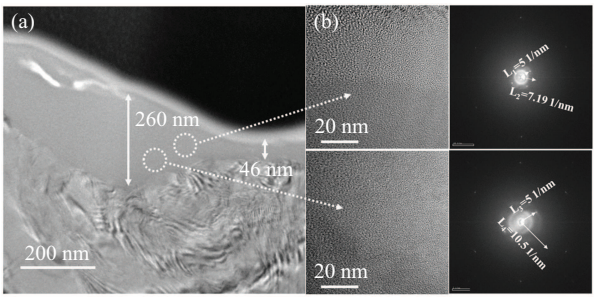


Fig. 3. (a) Bright field cross-sectional TEM image of DWS silicon wafer surface. (b) Partially enlarged views and corresponding electron diffraction pattern of areas shown in (a).

To further ascertain the components of the surface layer, bright field cross-sectional TEM images of DWS silicon wafer surface were obtained, as shown in Fig. 3. The thickness of the surface layer is about 46 nm in region A while is around 260 nm in region B, which is consistent with the Raman results shown in Fig. 2. From the partially enlarged views of the marked area in Fig. 3(a), only some nanocrystals can be observed. The diffraction rings can be indexed with Si-XII and Si-IV phases.[33,34] The grain size of Si-III phase may be too small or even amorphous to be detected.

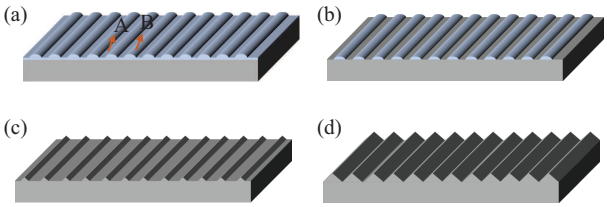


Fig. 4. Schematic diagram of the formation process of V-groove. (a) Surface of the DWS silicon wafers. (b) The critical state where the surface layer of area A is completely etched. (c) Small pyramids nucleating along the B region and connecting into lines. (d) Final V-groove structure.

Based on the investigations, the etching mechanism of V-groove in alkaline solution is proposed in the schematic diagram in Fig. 4. Figure 4(a) shows that the silicon wafer surface is composed of region A with a thinner surface layer and region B with a thicker surface layer. When the silicon wafer is etched in alkaline solution for less than 60 s, the surface layer in region A is completely removed and Si-I substrate is exposed (Fig. 4(b)). The etching rate of surface layer is made to be much lower than Si-I especially in the presence of the hypochlorite additive, which makes the surface layer behave like a mask. Therefore, the Si (100) in region A is etched away by following the etching rules of alkali solution, while the Si substrate underneath surface layer in region B stays intact. As the reaction progresses, the edges of region B are etched gradually, forming the ridge of V-groove. After that, even though the surface layer is completely removed, the etching reaction tends to follow the previous etching direction, thereby contributing to the growth of the V-groove.

3.2. Quasi-omnidirectionality of V-groove solar cells

The morphology SEM images of V-groove and pyramid wafer are shown in Fig. 5(a). It can be seen that the grooves are arranged regularly with a width of ~ 2 μm, while pyramids are distributed randomly in a large range of 0.5–5 μm, which, the improved uniformity of texture, would be beneficial towards the electrical performance of solar cells. In order to study the omnidirectionality of the V-groove texture, the reflectivity of V-groove under varying incident angles was simulated. AOI (θ) was defined as the angle between the incident direction and the normal of the silicon wafer. Notably, since the V-groove texture possesses excellent omnidirectional characteristics only in the case of incidence light parallel to the V-grooves,[15] the default incident light was in the normal plane of the silicon substrate. Simulation reflectivity results with the increased θ of V-groove and pyramid textured wafers are shown in Fig. S1. These results indicate that with the increase of θ, the reflectivity of the V-groove textured wafer remains almost unchanged with only a visible change at 75°, as shown in Fig. S1a. However, the reflectivity of the pyramid textured wafer increases significantly when θ increases, as is evident in Fig. S1b. More specifically, the calculated average reflectance based on the simulation results clearly reveals that the mean reflectance of the V-groove wafer remains around 15.6% with θ varying between 0° and 60° and slightly increases to 19.94% when θ is increased to 75°; while the mean reflectivity of the pyramid wafer increases significantly from 12.69% to 31.32% with θ varied from 0° and 75° (Fig. 5(b)). In addition, although the reflectivity of the V-groove texture is slightly higher than that of the pyramid texture at 0°, it is still very effective in reducing the reflectance in the wavelength range 300–1200 nm due to multiple reflections of the incident light.[15]

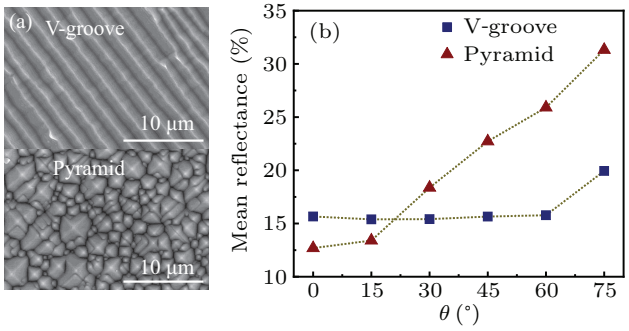


Fig. 5. (a) Morphology SEM images and (b) mean reflectance as a function of θ of V-groove and pyramid wafers.

The EQE of V-groove and pyramid solar cells under different θ was also measured, as shown in Figs. 6(a) and 6(b), respectively. The EQE of both V-groove and pyramid solar cells is found to decrease with the increase of θ. However, EQE of V-groove solar cells exhibits a more gradual decrease as compared to that of the pyramid solar cells and still maintains higher than 90% in the wavelength range of 500–950 nm under 75° incident light. What's more, the optical photographs of V-groove and pyramid solar cells as shown in Fig. S2 present that the V-groove solar cells look darker when imaged at a tilted angle, indicating superior omnidirectional characteristics of the V-groove solar cells. In order to further compare the omnidirectional difference between these two groups, the short-circuit current density (J_{sc}) can be calculated by

$$J_{sc,i} = q\int_{300\ \mathrm{nm}}^{1100\ \mathrm{nm}} \mathrm{EQE}(\lambda)\Gamma(\lambda)\mathrm{d}\lambda, \tag{1}$$

where i is the V-groove textured solar cell or pyramid textured solar cell, q is the electron charge, λ is the wavelength, $\mathrm{EQE}(\lambda)$ and $\Gamma(\lambda)$ represent the experimental EQE and the standard AM1.5 solar photon spectral distribution, respectively. The results are plotted in Fig. S2b. In the case of vertical incidence, $J_{sc,\mathrm{V-groove}}$ is slightly lower than that of pyramid solar cell, while with the increase of θ, $J_{sc,\mathrm{V-groove}}$ catches up with and even exceeds that of pyramid solar cell. Thus, it can be concluded that the V-groove solar cells possess superior quasi-omnidirectionality with slower change of reflectivity, EQE and J_{sc} when θ increases from 0° to 75°.

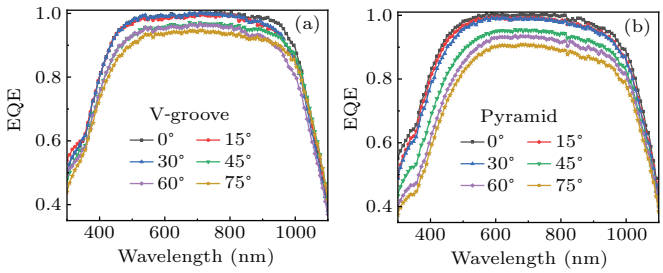


Fig. 6. EQE spectra for various angles of (a) V-groove-textured and (b) pyramid-textured solar cells.

3.3. Photovoltaic performances of V-groove solar cells

The τ_{eff} of V-groove and pyramid textures was measured after depositing 80 nm SiN_x:H films on both sides of silicon wafers symmetrically followed by annealing at 840 °C (Fig. 7(a)). It is obvious that the V-groove samples possess higher τ_{eff} due to the fact that the V-groove texture possesses fewer edges and thus fewer dangling bonds on the surface than the pyramid texture as shown in Fig. S3. At the injected carrier density (Δn) of 1×10^{14} cm^{-3}, the maximum τ_{eff} of the V-groove and pyramid samples are 162.4 μs and 114.6 μs, respectively. Therefore, surface recombination velocity S_{eff} can be calculated according to the following equation:[35]

$$\frac{1}{\tau_{\mathrm{eff}}} = \frac{1}{\tau_{\mathrm{bulk}}} + \frac{2S_{\mathrm{eff}}}{W}, \tag{2}$$

where W and τ_{bulk} are the wafer thickness (170 μm) and the bulk minority carrier lifetime, respectively. Here, $1/\tau_{\mathrm{bulk}}$ is small enough to be ignored. Thus, $S_{\mathrm{eff,V-groove}}$ and $S_{\mathrm{eff,pyramid}}$ can be calculated to be 52.3 cm/s and 74.2 cm/s, respectively.

In order to evaluate the quality of emitters formed on the two textured surfaces, emitter saturation current density J_{0e} is extracted according to the following equation:[36]

$$\frac{1}{\tau_{\mathrm{eff}}} - \frac{1}{\tau_{\mathrm{Auger}}} = \frac{1}{\tau_{\mathrm{SRH}}} + \frac{2J_{0e}}{qn_i^2W}(N_{\mathrm{dop}} + \Delta n), \tag{3}$$

where τ_{Auger} and τ_{SRH} represent the minority carrier lifetimes related to Auger recombination and Shockley–Read–Hall recombination, respectively. q is the basic charge, n_i is the intrinsic carrier density, and N_{dop} is the doping concentration of the silicon wafer. $1/\tau_{\mathrm{eff}} - 1/\tau_{\mathrm{Auger}}$ as a function of Δn is shown in Fig. 7(b). According to the slope of the line in Fig. 7(b), J_{0e} is calculated to be 39.7 fA/cm^2 and 31.2 fA/cm^2 for pyramid and V-groove, respectively, indicating a lower carrier recombination in the emitter for the V-groove texture. In addition, the measured applied FF is 86.9% for the V-groove sample and 86.7% for the pyramid sample, which is attributed to the reduced surface recombination and lower carrier recombination in the emitter of the V-groove sample. Based on these results, it can be concluded that the V-groove texture offers a higher ability to reduce the recombination of surface and emitter.

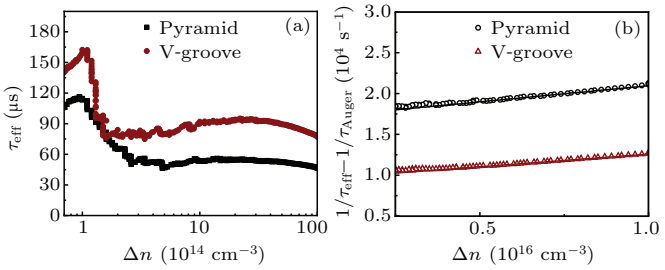


Fig. 7. (a) The τ_{eff} of pyramid and V-groove samples symmetrically passivated by SiN_x:H film. (b) $1/\tau_{\mathrm{eff}} - 1/\tau_{\mathrm{Auger}}$ results and their linear fits of pyramid and V-groove samples symmetrically passivated by SiN_x:H film.

SEM images of screen-printed Ag fingers parallel and perpendicular to the V-groove, and on pyramid texture after firing process are shown in Figs. 8 and S4. The widths of the Ag fingers of the V-groove are quite different in the case of parallel and perpendicular configurations, which are 35.5 μm and 52.3 μm, respectively. The corresponding width of the Ag fingers for the pyramid texture is 43.1 μm. The size of Ag particles in Ag paste is mainly distributed in the range of 1.1–3.72 μm,[1] which is comparable to the sizes of pyramids and V-grooves. When the Ag paste is pressed by a squeegee during screen-printing, it can easily spread through the gaps between the random pyramids. In the case of V-groove solar cell, when the fingers are in the direction of V-groove, the lateral flow of

Ag particles is hindered, which results in the minimum electrode width. When the fingers are perpendicular to V-groove, wider Ag fingers are obtained since there is a lower barrier for Ag particles to spread through. Due to the Ag busbars being much wider ($\sim$ 127 μm) than those fingers in a typical 9 busbars screen mask, the influence of texture on the busbar width is negligible. In addition, as shown in the enlarged views in Figs. 8 and S4, Ag particles can be found near the Ag fingers caused by Ag electrode contraction during sintering,[1] which can damage the emitter and result in poor surface passivation, causing a lowering of the circuit voltage (V_{oc}) and filling factor (FF). The widths of such regions are 7 μm, 17.5 μm and 10.3 μm, respectively for fingers parallel to the V-groove, perpendicular to the V-groove and on the pyramid, demonstrating the advantage of V-groove with parallel Ag fingers. Thus, the fingers were designed in parallel to the V-groove texture during the screen printing for the fabrication of the solar cells.

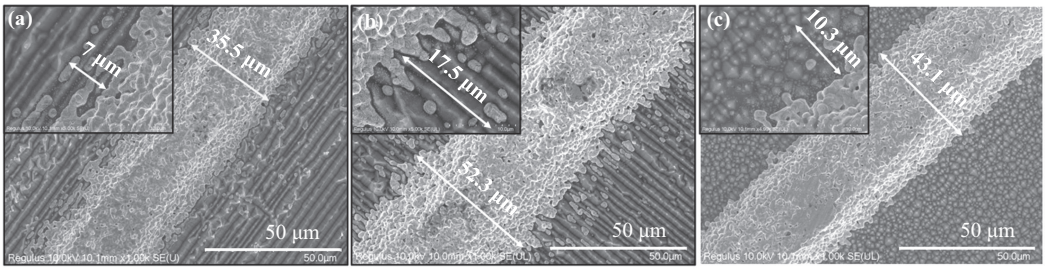


Fig. 8. SEM images and partially enlarged views of screen-printed Ag fingers (a) parallel to the V-groove, (b) perpendicular to the V-groove and (c) on pyramid texture after firing process.

The average photovoltaic performances of solar cells textured by V-groove and pyramid are listed in Table 1. As expected, the V-groove textured solar cells had higher J_{sc} due to the reduced shadowing area. The longer τ_{eff} and less damaged area together led to higher V_{oc} and FF. Finally, an average efficiency of 21.78% was achieved for the V-groove textured solar cells, which was 0.14% higher than the pyramid textured solar cells.

Table 1. The average photovoltaic parameters of 20 pyramid and V-groove solar cells.

	V_{oc} (mV)	J_{sc} (mA/cm^2)	FF (%)	η (%)
Pyramid	668.1	39.92	81.12	21.64
V-groove	669.9	40.01	81.27	21.78

The power generation (P_G) of V-groove textured solar cells and pyramid textured solar cells was calculated for both solar cells in one day and one year at Songshan Lake Materials Laboratory, respectively. The spectral irradiance as a function of wavelength at different time on June 21st is shown in Fig. 9(a). The P_G is calculated by the following formula:[3]

$$P_G(\theta) = V_{oc}(\theta) J_{sc}(\theta) FF. \tag{4}$$

Neglecting the effect of temperature, $J_{sc}(\theta)$ can be calculated by

$$J_{sc}(\theta) = q \int \mathrm{EQE}(\lambda, \theta) \Gamma(\lambda, \theta) \cos\theta \, \mathrm{d}\lambda, \tag{5}$$

where $\Gamma(\lambda, \theta)$ is the incident photo flux. $V_{oc}(\theta)$ is obtained from the following Shockley equation:[3]

$$V_{oc} \approx \frac{kT}{q} \ln\left(\frac{J_{sc}(\theta)}{J_0} + 1\right), \tag{6}$$

where k is the Boltzmann constant, T is the thermodynamic temperature, and J_0 is the saturated current density. Ideally, the fill factor FF is only a function of the open-circuit voltage V_{oc}

$$FF = \frac{\frac{qV_{oc}}{kT} - \ln\left(\frac{qV_{oc}}{kT} + 0.72\right)}{\frac{qV_{oc}}{kT} + 1}. \tag{7}$$

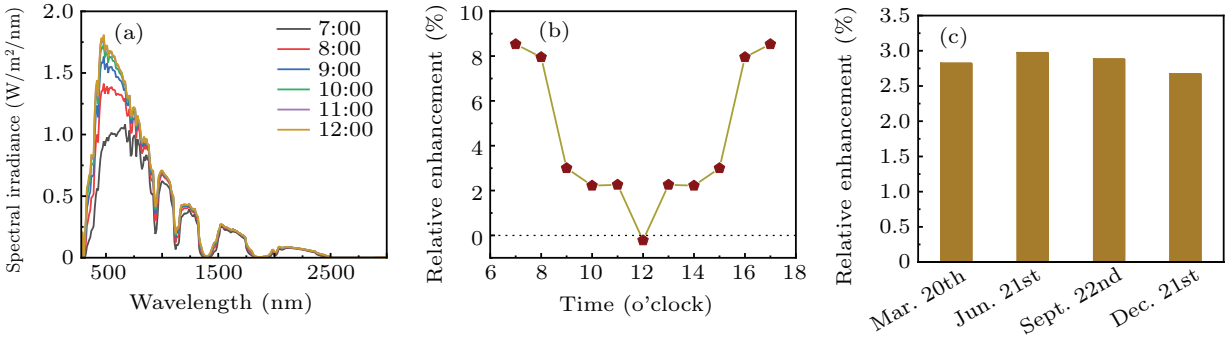


Fig. 9. (a) Simulated solar spectral irradiance varying with time on June 21st, 2022, Songshan Lake Materials Laboratory (latitude of 22.9°, longitude 113.87°). (b) Relative enhancement of the P_{out} of V-groove-textured solar cells as a function of time on June 21st, at Songshan Lake Materials Laboratory. (c) Relative enhancement of energy output of V-groove solar cells on March 20th, June 21st, September 22nd, and December 21st, 2022, at Songshan Lake Materials Laboratory.

The calculated enhancement of P_G of the V-groove textured solar cells compared to the pyramid textured solar cells in one day and one year is shown in Figs. 9(b) and 9(c), respectively. On June 21st in Songshan Lake Materials Laboratory, the P_G of the V-groove textured solar cells is obviously higher than that of the pyramid textured solar cell except at 12:00 pm when θ is 0° at which it is only slightly lower. At 7:00 am and 15:00 pm, the relative enhancement of the V-groove textured solar cells even reaches 8.75%. To simplify the calculation of one year, one representative day is chosen for each season, namely, March 20th, June 21st, September 22nd, and December 21st. As shown in Fig. 9(c), the P_G of the V-groove textured solar cells steadily exceeds that of the pyramid solar cell at each representative day. The highest relative enhancement (2.97%) is achieved in the summer while the lowest enhancement (2.67%) is obtained in the winter. Generally, a 2.84% enhancement can be expected every year when replacing traditional pyramid texture by V-groove texture, which is quite a considerable improvement.

4. Conclusion and perspectives

In summary, V-groove texture surrounded by {111} surfaces was fabricated utilizing the natural mask on diamond wire-sawn silicon wafer and an in-house developed additive during alkaline solution etching, providing an economical and scalable preparation method for industrial application. Compared with the typical pyramid texture, the V-groove texture has excellent quasi-omnidirectionality within light incidence angles of 0°–75°. Benefiting from the higher τ_{eff}, lower surface damage at electrode edges and reduced shading area of front Ag electrodes, the V-groove textured solar cells obtained higher V_{oc}, FF and J_{sc} compared to traditional pyramid textured solar cells. The average efficiency of the V-groove solar cells was 21.78%, which was 0.14% higher than that of the pyramid solar cells. Aided by the excellent quasi-omnidirectionality of V-groove texture, an appreciable enhancement of 2.84% in power generation can be expected for one year, which exhibits a wide application prospect.

Acknowledgements

Project supported by the Key-Area Research and Development Program of Guangdong Province, China (Grant No. 2021B0101260001), Guangdong Basic and Applied Basic Research Foundation (Grant No. 2019A1515110411), the National Natural Science Foundation of China (Grant No. 61904201).

References

[1] Ju M, Mallem K, Dutta S, Balaji N, Oh D, Cho E C, Cho Y H, Kim Y and Yi J 2018 *Materials Science in Semiconductor Processing* **85** 68
[2] Wang J, Zhong F, Liu H, Zhao L, Wang W, Xu X, Zhang Y and Yan H 2021 *Solar Energy* **221** 114
[3] Zhong S, Wang W, Tan M, Zhuang Y and Shen W 2017 *Advanced Science* **4** 1700200
[4] Bazyari S, Keypour R, Farhangi S, Ghaedi A and Bazyari K 2014 *Journal of Power and Energy Engineering* **02** 718
[5] Spinelli P, Verschuuren M A and Polman A 2012 *Nat. Commun.* **3** 692
[6] Yang L, Mo L, Okuno Y and He S 2013 *Progress in Photovoltaics: Research and Applications* **21** 1077
[7] Xu Z, Yao Y, Brueckner E P, Li L, Jiang J, Nuzzo R G and Liu G L 2014 *Nanotechnology* **25** 305301
[8] Zhuang Y F, Zhong S H, Xu H Y and Shen W Z 2018 *Solar Energy Materials and Solar Cells* **179** 372
[9] Li Y, Zhong S, Zhuang Y, Yang L, Meng F, Wang W, Li Z and Shen W 2019 *Advanced Electronic Materials* **5** 1800858
[10] Zhong S and Shen W 2020 *J. Phys. D: Appl. Phys.* **53** 483001
[11] Lee I J, Paik U and Park J G 2013 *Solar Energy* **91** 256
[12] Oh J, Yuan H C and Branz H M 2012 *Nat. Nanotechnol.* **7** 743
[13] Toor F, Oh J and Branz H M 2014 *Progress in Photovoltaics: Research and Applications* **23** 1375
[14] Savin H, Repo P, Gastrow G, Ortega P, Calle E, Garin M and Alcubilla R 2015 *Nat. Nanotechnol.* **10** 624
[15] Zhan Y, Liu Y, Chen Q, Chen W, Wu J, Wang Y and Du X 2019 *Solar Energy* **193** 132
[16] Zhao Y, Liu Y, Chen W, Wu J, Chen Q, Tang H, Wang Y and Du X 2020 *Solar Energy* **201** 461
[17] Blakers A W and Green M A 1986 *Appl. Phys. Lett.* **48** 215
[18] Reddeppa M, Thota C, Nam D J, Woo H, Kim S G and Kim M D 2021 *Appl. Phys. Lett.* **119** 023901
[19] Gerhards C, Marckmann C, Tolle R, Spiegel M, Fath P, Willeke G, Bucher E, Creager J and Narayanan S 1997 *the Twenty Sixth IEEE Photovoltaic Specialists Conference,* 29 September–03 October, 1997, Anaheim CA, USA, p. 43
[20] Fath P, Borst C, Zechner C, Bucher E, Willeke G and Narayanan S 1997 *Solar Energy Materials and Solar Cells* **48** 229
[21] Untila G, Palov A, Kost T, Chebotareva A, Stepanov A, Zaks M, Sitnikov A, Saprykin D and Grishaev A 2013 *Physica Status Solidi (a)* **210** 760
[22] Cho C, Kim H, Jeong S, Baek S W, Seo J W, Han D, Kim K, Park Y, Yoo S and Lee J Y 2013 *Solar Energy Materials and Solar Cells* **115** 36
[23] Chappell T I The V-groove multijunction solar cell 1979 *IEEE Transactions on Electron Devices*, July 1979, **26** p. 1091
[24] Domnich V, Gogotsi Y and Dub S 2000 *Appl. Phys. Lett.* **76** 2214
[25] Kailer A, Gogotsi Y G and Nickel K G 1997 *J. Appl. Phys.* **81** 3057
[26] Bradby J E, Williams J S and Swain M V 2003 *Phys. Rev. B* **67** 085205
[27] Bradby J E, Williams J S, Wong-Leung J, Swain M V and Munroe P 2000 *Appl. Phys. Lett.* **77** 3749
[28] Xu X, Wang P, Li X and Yang D 2012 *Solar Energy Materials and Solar Cells* **98** 337
[29] Kawasegi N, Morita N, Yamada S, Takano N, Oyama T and Ashida K 2005 *Nanotechnology* **16** 1411
[30] Chen W, Liu Y, Yang L, Wu J, Chen Q, Zhao Y, Wang Y and Du X 2018 *Sci. Rep.* **8** 3408
[31] Lee D B 1969 *J. Appl. Phys.* **40** 4569
[32] Seidel H, Csepregi L, Heuberger A and Baumgartel H 1990 *Journal of the Electrochemical Society* **137** 3612
[33] Liang T, Xiong L, Lou H, Lan F, Zhang J, Liu Y, Li D, Zeng Q and Zeng Z 2022 *Scripta Materialia* **220** 114936
[34] Ikoma Y 2019 *Materials Transactions* **60** 1168
[35] Sproul A B 1994 *J. Appl. Phys.* **76** 2851
[36] Wang F, Zhang Y, Yang M, Yang L, Sui Y, Yang J, Zhao Y and Zhang X 2018 *Advanced Functional Materials* **28** 1805001